J Ther Eng, Vol. 12, No. 2, pp. 595−609, March, 2026

Journal of Thermal Engineering
Web page info: https://jten.yildiz.edu.tr
DOI: 10.14744/thermal.0001103

Journal of Thermal Engineering

Research Article

Investigation of thermal and hydrodynamic performance of a plate compact heat exchanger with Levenberg-Marquardt artificial neural network method

Aykut BACAK[1]

[1]*ASELSAN INC., Golbasi Yerleskesi, Ankara, 06830, Turkiye*

ARTICLE INFO

Article history
Received: 06 March 2024
Revised: 20 April 2024
Accepted: 26 April 2024

Keywords:
Artificial Neural Network; Compact Heat Exchanger; Heat Transfer Coefficient; Levenberg-Marquardt; Pressure Drop

ABSTRACT

Compact heat exchangers are an essential device for efficiently transferring thermal energy between fluids. In contrast to larger objects of the same kind, they do this by optimizing the surface area for heat transmission inside a more compact space. This study theoretically calculates the heat transfer coefficient and pressure drop of a plate compact heat exchanger using design parameters such as air flow rate (1-4 kg/s), inlet air temperature (300-350 K), outlet air temperature (400-450 K), passage width (0.003-0.05 m), divider width (0.001-0.005 m), and heat exchanger length (0.15-1 m) at atmospheric pressure (101325 Pa). The study uses the Levenberg-Marquardt artificial neural network method to investigate heat transfer coefficients in compact heat exchangers. Results demonstration that the coefficient increases with mass flow rate doubling and 93% tripling. The maximum coefficient increases by 7.9% with a divider width of 0.001 m, while it decreases with shorter route lengths. The investigation revealed that pressure decreases exhibit a more pronounced rise in relation to the width of the divider. The factors increased by 1.04, 1.08, 1.13, 1.17, and 1.22 for divider widths of 0.001 m and 0.005 m, respectively, at varying temperatures. The change in the width of the divider had little effect on the pressure decrease at constant average temperatures. The Mean Squared Error (MSE) for heat transfer was -0.1787, whereas the MSE for pressure drop was 3.988. The training phase of the ANN was flawless, achieving projected values over 200 W/m^{2}K and a pressure decrease surpassing 5000 Pa.

Cite this article as: Bacak A. Investigation of thermal and hydrodynamic performance of a plate compact heat exchanger with Levenberg-Marquardt artificial neural network method. J Ther Eng 2026;12(2):595−609.

INTRODUCTION

Plate-fin heat exchangers (PFHE) are utilized widely and frequently in the heating, cooling, air conditioning, power generation, and heat recovery industries. In these fields, heat exchangers (HEX) are complicated systems that depend on design factors like the width of the divider, the passage, the air temperature, the atmospheric pressure, and the mass flow rate. It is difficult to predict the movement

***Corresponding author.**
*E-mail address: bacakaykut@gmail.com

This paper was recommended for publication in revised form by Editor-in Chief Ahmet Selim Dalkilic

of heat and the reduction of pressure in various fin types utilized in PFHEs, including plain, wavy, serrated, perforated, and louvered fins. Because there are so many geometric parameters, there isn't a lot of experimental data in the literature. Because of this, some experimental correlations were used to make an educated guess about how well the fin would work in PFHEs. Most people think that mistakes in estimating caused by correlations are much worse than mistakes in measuring, mostly because they involve compressing data. Currently, artificial neural networks (ANN) are utilized to address the challenge of forecasting the thermal characteristics of various HEXs.

The literature review undertaken in this article is examined in three segments: investigations into thermal performance utilizing ANN methodologies, research aimed at enhancing thermal and hydrodynamic efficiency, and thermo-economic analyses. The studies in the literature on thermal effects are summarized in the following paragraph. Ermis [1] uses ANN to look at how heat moves through small HEXs. The ANN uses experimental data to guess the heat transfer coefficient (HTC), the pressure drops (ΔP), and the Nusselt number. The network uses a feed-forward back-propagation algorithm and various hidden numbers to predict heat transfer values. The trained ANN outperforms experimental results, with an absolute mean relative error of less than 6%. Demir [2] uses an ANN model to pretend the thermal performance of a chevron-type plate HEX using water as the operating fluid. The model estimates outer temperatures based on cold water mass flow rate, inlet hot water temperature, and inlet cold water temperature, employing partial data. The experimental and predicted results are very close to each other. The network predicts outlet temperatures of 2.58% for hot water and 1.80% for cold water. Shi et al. [3] examine the equivalent thermal conduction resistance of printed circuit heat exchangers (PCHE) and their impact on thermal convection resistance. The consequences show that PCHEs with unequal numbers of hot and cold plates have a sensitive equivalent thermal conduction resistance, with a maximum value of 1.7–2.4 times the smallest value. The proposed correlations have acceptable accuracy for overall engineering claims. The ANN model is better at making predictions, so it is recommended for important needs. Dossumbekov et al. [4] aims to develop models for calculating the Nusselt number in a micro-HEX utilizing hybrid nanofluids through advanced methodologies. This research utilizes experimental data from a different study to suggest models based on multilayer perceptron (MLP) and Group Method of Data Handling (GMDH) neural networks (NN). The models are very accurate, with R2 values of 0.9948 and 0.9972, correspondingly. The overall Absolute Relative Deviation (AARD) of the studies is 2.43% and 1.56%, respectively. Li et al. [5] emphasize optimizing the thermal hydraulic performance of a PCHE for the supercritical carbon dioxide (S-CO_2) Brayton cycle. The four parameters that were chosen were the airfoil fin's maximum thickness, maximum thickness location, transverse pitch, and staggered pitch. The study used computational fluid dynamics (CFD) simulations, machine learning, and optimization algorithms. Results presented that growing the extreme thickness location value improved the PCHE's performance by about 6.2% associated with the basic structure. The study also used the sequential quadratic programming (SQP) algorithm and non-dominated sorting genetic algorithm II (NSGA-II) for optimization. Zhu et al. [6] propose experimental systems for two-phase flow heat transfer in mini channels utilizing ANN models. The models forecast heat transfer performance acceptably with a Mean Absolute Relative Deviation (MARD) of 11.41% and 6.06%, respectively. The ANN study can be transferred across various datasets but demonstrations unacceptable performance for various situations. This study can benefit advanced thermal management systems. Zarea et al. [7] utilize the Bees Algorithm (BA) in the model of a cross-flow plate-fin HEX with an offset strip fin. The algorithm is optimized using the second law of thermodynamics and minimizes entropy generation units. The study compares BA's effectiveness and accuracy with other algorithms like GA, Particle Swarm Optimization (PSO), Imperialist Competitive Algorithm (ICA), and initial project. The results display BA offers higher accuracy in finding the optimum configuration. Hernández-Gil et al. [8] employ an ANN and mathematical approaches to compute the heat transfer area, considering the nonlinear fluctuations of the global HTC due to fluid properties and surface geometry. The method was tested in two different situations, and the results showed that it could predict the heat transfer area with an error rate of less than 2.8%. Zeng et al. [9] investigate the ΔP and heat transfer characteristics of a high-efficiency plate-fin structure in an air preheater, focusing on the critical Reynolds number for turbulent flow conversion and separating HTCs using the Genetic Algorithm method. The findings will aid in the in the future design of high-efficiency heat preheaters. Gupta et al. [10] developed an ANN model to predict the performance parameters of perforated micro-pin fin heat sinks under different geometric parameters and inflow circumstances. A 3-D CFD simulation system was used to produce dataset examples. The model forecasts the Nusselt number and friction factor with a mean absolute percentage error (MAPE) of 4.45% and 1.80%, correspondingly. A multi-objective non-dominated sorting genetic algorithm (NSGA-II) was employed for optimization, resulting in an increase in thermal performance between 11.5% and 39.77%.

The studies in the literature where thermal and hydrodynamic effects are examined together are summarized in the following paragraph. Peng and Lin [11] dynamically optimized the Support Vector Regression (SVR) model to the research method, and k-fold cross-validation was projected to forecast the thermal-hydraulic performance of compact heat exchangers (CHEs). The model's performance was evaluated with 48 experimental data points and

associated with the ANN method. The SVR model showed better estimate performance with mean squared errors (MSE) of 2.645×10^{-4} for testing the j factor and 1.231×10^{-3} for testing the f factor. Peng and Lin [12] present an application of ANNs to forecast ΔP and heat transfer characteristics in PFHEs. The research assesses the thermal efficiencies of five PFHEs and constructs a feed-forward neural network utilizing a backpropagation algorithm. The ANN is trained on experimental data to predict the j and f factors in PFHEs. It gets MSEs of less than 1.5% for the j factor and 1% for the f factor. Nascimento et al. [13] employ an optimization technique and a Random Vector Functional Link (RVFL) network to develop a counter-flow PFHE featuring offset-strip fins. CFD simulations created a dataset for training and testing, thereby reducing processing time and ensuring the accuracy of PFHE. The Non-Dominated Sorting Genetic Algorithm III (NSGA-III) was computed to accomplish optimal effectiveness, minimal volume, and ΔP at both the hot and cold sides. Experimental endorsement employing the Shear Stress Transport (SST) k-ω turbulence model indicated 4.36% and 3.27% discrepancies in ΔP and convective HTC measurements, respectively. Singh et al. [14] suggest employing Response Surface Methodology (RSM) and ANN to optimize the design of fin-tube heat exchangers (FTHEs) equipped with vortex generators. The ANN was better at forecasting the Nusselt number and friction factor than the RSM, with R-squared values of 0.990 and 0.954. The best design configurations were recommended based on how well they exchanged heat or lowered ΔP, making sure that both goals were met in a balanced way.

The studies in the literature where thermo-economic analysis is examined in conjunction with the ANN method are summarized in the following paragraph. Xie et al. [15] concentrate on enhancing a plate-fin type CHE through the application of a GA. The GA searches, combines, and optimizes structure sizes, with the minimum total volume and yearly price as objective functions. The fin geometries are fixed, and three shape parameters are varied with or without ΔP constraints. The improved CHE offers 30% lesser volume or 15% lower yearly price with ΔP constraints and 49% lower volume or 16% lower annual cost without ΔP constraints. Jilak et al. [16] optimize a plate HEX design employing a multi-objective evolutionary algorithm/decomposition, considering thermal efficiency and manufacturing cost as objective functions. The ε-NTU method was utilized to look at the chances of ΔP and efficiency. A ceramics factory in Kerman Province did an experiment and found that the expected design led to a 19.962% increase in efficacy rate and a 9.533% decrease in price. We used Pareto front analysis to show how the best points for design variables are spread out. Peng and Lin [17] demonstrate the efficacy of GA and Backpropagation Neural Networks (BP) in enhancing PFHE. The main objectives are minimizing total weight and annual cost, ensuring the smallest size with minimal capital cost, and maximizing ΔPs. The GA combined with the BP method optimizes variables such as core length, number of hot side layers, fin height, and pitch, making this method universally applicable for various PFHEs.

The literature research indicated that ANNs are more effective for thermal analysis in engineering applications, particularly in HEXs. The Levenberg-Marquardt ANN method has not yet been utilized or evaluated for thermal properties in PFHE. This paper's investigation focuses on examining the effectiveness of ANN with the Levenberg-Marquardt method in analyzing thermal features (such as ΔP and heat transfer) in a PFHE. A theoretical calculation was established to study the thermal performance of PFHE. The theoretical data was analyzed using the ANN approach to demonstrate its effectiveness in representing design parameters. A methodology utilizing cross-validation was created to evaluate the anticipated inaccuracy of the ANN method built from insufficient data in predicting PFHEs behavior under various operating situations and design parameters. With this study, it has been determined that compact heat exchangers produce solutions within a very low deviation range of ±10, and solutions are provided in a short time with ANN management without requiring additional experimental work and thermal analysis. As can be seen from the literature studies, the Levenberg-Marquardt ANN method has almost never been used in compact heat exchanger studies, and this study takes its place in the literature as a guide for compact heat exchanger designers, manufacturers, and researchers.

THERMAL CALCULATION

The thermal and hydrodynamic performance of the Compact HEX as shown in Figure 1 was analyzed by calculating the HTC and pressure loss using EES V9.944 software. The e-NTU method was utilized to determine the heat transfer capability of the compact HEX. The thermal and hydrodynamic calculations of the compact heat exchanger are calculated as shown in equations (1) to (14) [18].

The effectiveness of a cross-flow HEX with distinct fluids as proposed:

$$\varepsilon = \frac{q}{q_{\max}} = \frac{C_h\left(T_{h,in} - T_{h,out}\right)}{C_{\min}\left(T_{h,in} - T_{h,out}\right)} = \frac{C_c\left(T_{c,out} - T_{c,in}\right)}{C_{\min}\left(T_{h,in} - T_{h,out}\right)} \quad (1)$$

where C_{min} is the lesser of the C_h and C_c magnitudes. NTU is calculated as follows:

$$NTU = \frac{AU_{Ave}}{C_{\min}} = \frac{1}{C_{\min}}\int_0^A UdA \quad (2)$$

where A is the heat transfer area as used in the description of U. In design work U can commonly be preserved as constant.

$$C^* = \frac{C_{\min}}{C_{\max}} \quad (3)$$

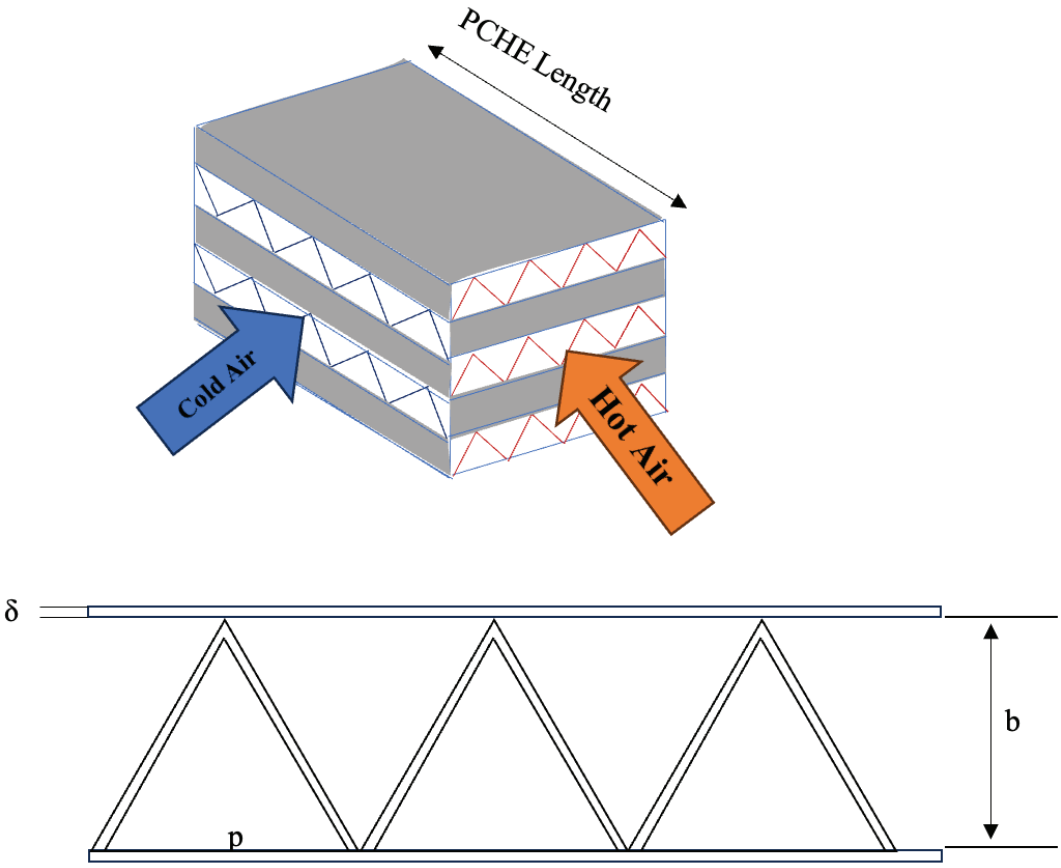

Figure 1. Geometry and design parameters.

where C_{min} and C_{max} are correspondingly, the lesser and the greater of the two magnitudes C_h and C_c.

U is the average HTC and A_{tot} is total heat transfer surface area calculated from:

$$\frac{1}{U_h}=\frac{1}{\eta_{o,h}h_h}+\frac{\alpha}{(A_w/A_h)k}+\frac{1}{(A_c/A_h)\eta_{o,c}h_c} \tag{4}$$

$$\frac{1}{U_c}=\frac{1}{\eta_{o,c}h_c}+\frac{\delta}{(A_w/A_c)k}+\frac{1}{(A_h/A_c)\eta_{o,h}h_h} \tag{5}$$

Where U_h is based on a unit of hot-side total area and Uc is based on a unit of cold-side total area. A_w signifies the overall wall area; $\eta_{c,h}$ and $\eta_{o,h}$ represent temperature effectiveness of the total area A_h and A_c, correspondingly.

$$\eta_o=1-\frac{A_{fr}}{A_{tot}}(1-\eta_f) \tag{6}$$

where A_f is the frontal area, A is the total area, η_f is number of fins and η_o is the weighted average of the 100% effectiveness of the prime surface. Gardner [19] gives relations for η_f for a number of fin geometries.

$$\eta_f=\frac{\tanh(ml)}{ml} \tag{7}$$

$$m=\sqrt{\frac{2h}{k\delta_f}} \tag{8}$$

where h is the HTC, k is the thermal conductivity, and δ is the fin thickness.

Mass flux, G, can be expressed as:

$$G=\frac{\dot{m}}{\sigma A_{fr}} \tag{9}$$

The variables are defined as follows: $\dot{m}$ represents the mass flow rate, σ is the ratio of the free flow area to the frontal area, and A_{fr} denotes the frontal area. Calculate the Reynold's number using the following formula:

$$\mathrm{Re}=\frac{GD_h}{\mu} \tag{10}$$

D_h represents the hydraulic diameter, μ stands for dynamic viscosity, and G is the result of multiplying

the maximum mass velocity by the density of the fluid. Hydraulic diameter is estimated as follows:

$$D_h = \frac{2a\left(b-\delta_f\right)}{a+2\left(l_f-\delta_f\right)} \tag{11}$$

The Colburn j_H factor which is a function of the Stanton the Prandtl number and is calculated as follows:

$$j_H = St\,\mathrm{Pr}^{2/3} \tag{12}$$

$$St = \frac{Nu}{\mathrm{Re\,Pr}} = \frac{h}{Gc_p} = \frac{q_w}{c_p G(T_m - T_w)} \tag{13}$$

Pressure Drop Calculation

Pressure drop in compact HEX is calculated as follows:

$$\frac{\Delta P}{P_{in}} = \frac{G^2}{2g_c}\frac{v_{in}}{P_{in}}\left[\left(1+\sigma^2\right)\left(\frac{v_{out}}{v_{in}}-1\right)+f\frac{A}{A_c}\frac{v_{ave}}{v_{in}}\right] \tag{14}$$

where σ is the ratio of minimum free flow area to frontal area and *f* is the Fanning friction factor.

ANN Model Development

An MLP-based ANN method has been established to estimate the HTC and ΔP of the compact HEX. MLP networks, which consist of interconnected layers, are one of the ANN models that can make predictions with high accuracy due to their strong systematic structure. Structurally, an MLP network contains an input layer, a hidden layer, and an output layer. Air flow rate, air temperature, passage width, and HEX length are described as shown in Table 1 as input parameters in the input layer of the developed MLP network. In the network model, the layer afterward the input layer is the hidden layer, and every MLP network has at least one hidden layer. The lack of a set way to calculate the neuron, which is an important part of the hidden layer, makes it hard for MLP networks to grow. To compute the number of neurons in the hidden layer, the most commonly used technique is to evaluate the performance of network models created with dissimilar neuron numbers. In the developed network model, performance analyses of MLP networks with numerous neuron numbers are made, and the model with 10 neurons in the hidden layer is selected. In the output layer, which is the next layer from the hidden layer, two different parameters are estimated, namely HTC and ΔP. Figure 2 presents the symbolic configuration scheme and basic architecture of the created MLP network. The machine-learning model has three stages: training, prediction, and validation. A specific part of the data in the study should be reserved for training. Training is the stage of teaching the available data to the machine. Prediction, on the other hand, is the stage of creating the machine's outputs that performs the learning from the data at hand. On the other hand, validation is the validation phase of the results obtained in the prediction phase with theoretical calculations. The ANN develops a total of 13860 data points, reserving 9702 for model training, 2079 for validation, and another 2079 for testing. As the training algorithm, the LM-type ANN training algorithm, which is frequently used in ANN models and has high learning ability, is preferred. Transfer functions are utilized in the hidden and output layers of the MLP network to estimate the HTC and ΔP, respectively. Table 2 contains info on how data is examined for ANN approaches.

To evaluate the approximation performance of the designed ANN method, coefficient of determination (R) and MSE parameters, which are extensively used in the previous studies, are selected. In addition to these performance parameters, the values of HTC and ΔP attained from the ANN method and the margin of deviation (MoD) values, which represent the relational deviation among the target ones, are also calculated. The statistical equations working in the computation of the performance factors are as indicate:

$$MSE = \frac{1}{N}\sum_{i=1}^{N}\left(X_{Calc(i)} - X_{ANN(i)}\right)^2 \tag{15}$$

Table 1. Input parameters for thermal and ANN calculation

	Symbol	Values	Unit
Mass Flow Rate	m	1-4	kg/s
Inlet Temperature	T_i	300-350	K
Outlet Temperature	T_o	400-450	K
Width of Passages for Second Fluid	b_2	0.003-0.05	m
Width of Divider	a	0.001-0.005	m
Atmospheric Pressure	P_{Atm}	101325	Pa
Length of Heat Exchanger	L	0.15-1	m

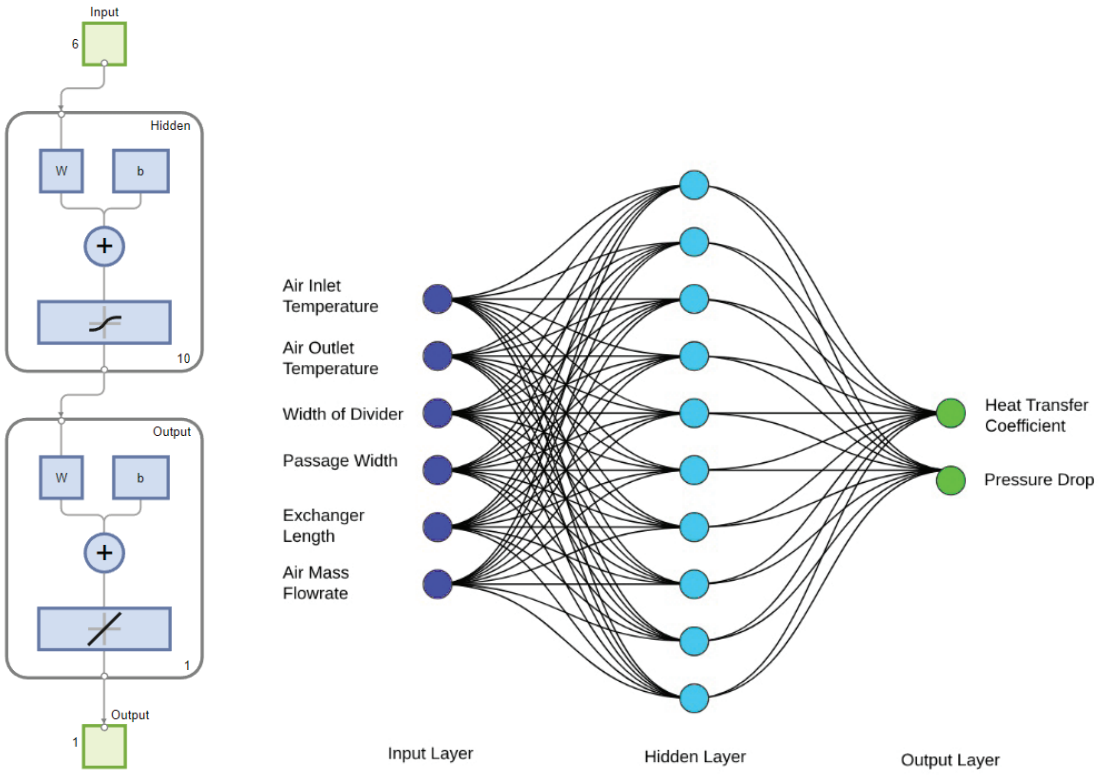

a) b)

Figure 2. The effectiveness of the training process of ANN architectures (a), and basic structural topology of an MLP network.

Table 2. Details of the estimated data for both ANN models

	Data Number				Number of Neuron
	Training	Validation	Test	Total	
for Heat Transfer Coefficient	9702	2079	2079	13860	10
for Pressure Drop	9702	2079	2079	13860	10

$$R = \sqrt{1 - \frac{\sum_{i=1}^{N} \left(X_{Calc(i)} - X_{ANN(i)} \right)^2}{\sum_{i=1}^{N} \left(X_{Calc(i)} \right)^2}} \quad (16)$$

The MoD values, which show how far off the predicted values are from the target values using the ANN, are also calculated and looked at with the performance parameters. These numbers show how far off the predicted values are from the target values. The accurate method utilized to find the MoD is shown below:

$$MoD(\%) = \left[\frac{X_{Calc} - X_{ANN}}{X_{Calc}} \right] x100 \quad (17)$$

RESULTS AND DISCUSSION

This study employs theoretical calculations to determine the heat transfer coefficient and pressure drop of a plate-compact heat exchanger. The design parameters considered include the air flow rate (ranging from 1 to 4 kg/s), inlet air temperature (ranging from 300 to 350 K), outlet air temperature (ranging from 400 to 450 K), passage width (ranging from 0.003 to 0.05 m), divider width (ranging from 0.001 to 0.005 m), and heat exchanger length (ranging from 0.15 to 1 m). The calculations are done at normal atmospheric pressure (101325 Pa). To research used the Levenberg-Marquardt artificial neural network technique to examine heat transfer coefficients in compact heat exchangers. Neither the theoretical nor the ANN study includes further experimental studies since the calculated

values are derived from a curve that accurately represents the experimental data of Kays and London [18].

Figure 3 shows how the total HTC changes based on different design parameters of small HEXs. Figure 3(a) displays the variation in HTC based on various HEX lengths ranging from 0.003 to 0.04 m and the width of the divider. The input and output air temperatures in the diagram are 300 K and 400 K, correspondingly, when figuring out the HTC. The air flow rate is 1 kg/s, and the length of the HEX is 1 m. Figure 3(a) shows that when the divider width grows, the HTC increases for all channel widths. The HTC increases by around 27.9% when the width of passages triples and by about 57.7% when the width of passages increases tenfold, as seen in the figure. A rise in the width of channels consequences in a growth in the heat transfer surface area, although this rise is not proportionate.

Figure 3(b) displays the change in the HTC value of the plate compact HEX based on the divider width and air mass flow rate parameters. The figure illustrates that the HTC value increases as the width of the divider value grows for all air mass flow rate values. For an air mass flow rate of 1 kg/s, the HTC value increases by 4.8%, 11.9%, 18.9%, and 26.1% when the width of the divider value increases by 2, 3, 4, and 5 times, respectively, as shown in the figure. When analyzing this perspective with an airflow rate of 3 kg/s, the rise rates are 7.2%, 14.3%, 21.7%, and 28.4%, respectively. At high mass flow rates, the HTC value grows more rapidly with the increase in the divider width. As the air flow rate increases, the HTC value rises. The figure shows that the HTC increases by an average of 51.3% with a doubling of the mass flow rate and by about 93% with a tripling of the mass flow rate. In compact HEXs, there is no direct relationship between mass flow rate and HTC. Figure 3(c) shows the change in HTC value for a plate compact HEX based on the divider width and average air temperature. The figure displays that the HTC value rises as the divider's breadth increases. At an average air temperature of 350 K, the HTC value increases by 4.8%, 11.9%, 19.2%, and 26.1% when the width of the divider value increases by 2, 3, 4, and 5 times. For an average temperature of 400 K, these values are 4.3%, 9.1%, 15.9%, and 22.7%, respectively. Higher temperatures result in slightly greater increases in the HTC compared to lower temperatures. As the average air temperature increases, the HTC value naturally increases. With a divider width of 0.001 m, the maximum HTC increases by 7.9%, compared to an increase of roughly 5% with a divider

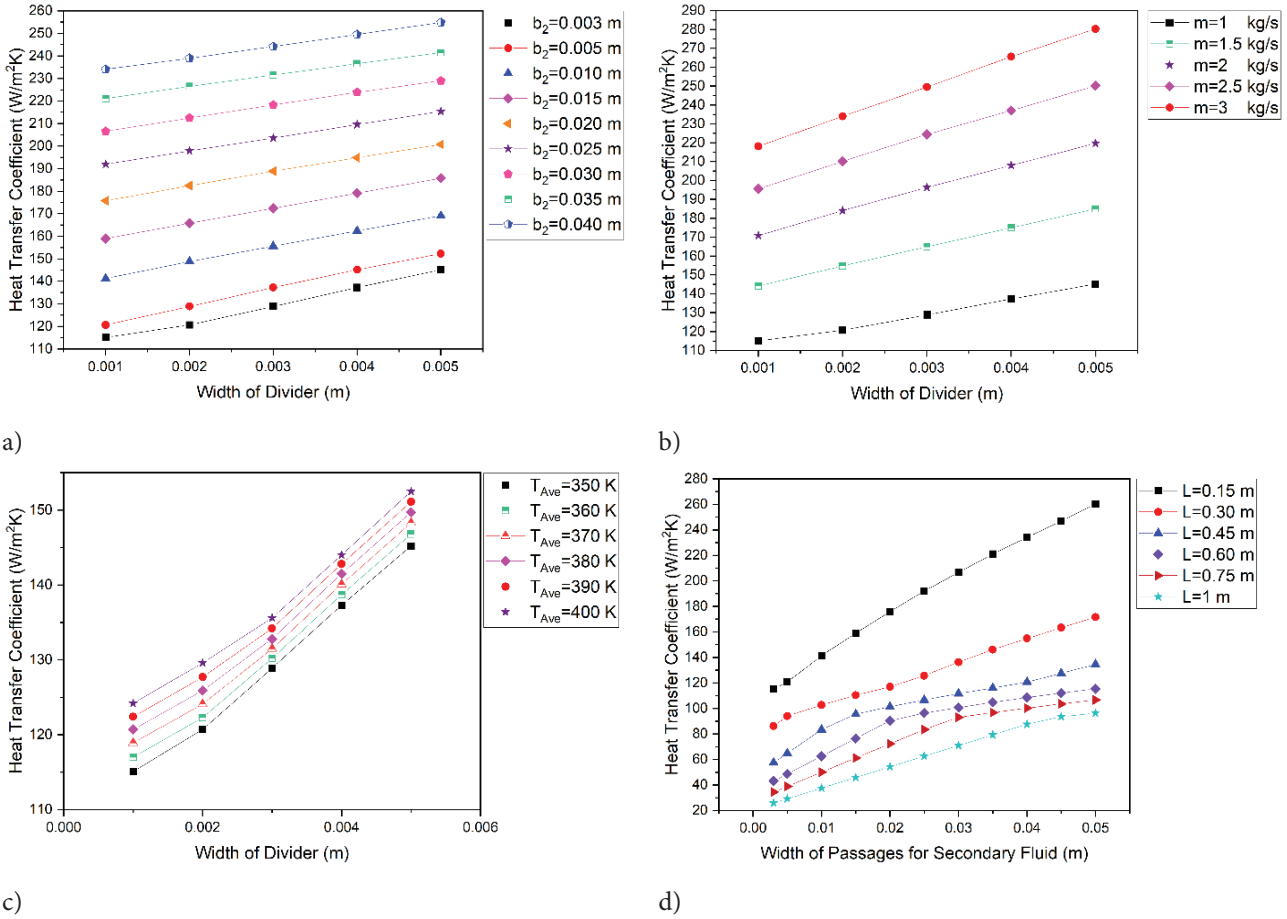

Figure 3. Heat transfer coefficient variation with respect to a) length of heat exchanger, b) mass flow rate, c) average temperature, and, d) width of passages for secondary fluid.

width of 0.005 m. An increase in the average temperature of compact HEXs with larger heat transfer areas leads to a gradual rise in the HTC at a slower rate.

Figure 3(d) shows how the HTC value of the plate compact HEX changes when the passageways are wider or the HEX is longer. When creating the figure, the divider width is 0.001 m, the air input temperature is 300K, the air exit temperature is 400K, and the air flow rate is 1 kg/s. The graphic illustrates that as the length of the compact HEX rises, the HTC value falls. With a passage width of 0.003 m, the HTC decreases by 80.2% when the exchanger length is raised from 0.15 m to 1 m. For a passage width of 0.05 m, this decline reduces to 53.8%. Increasing the length of the exchanger in wider channels results in a less significant decrease in the HTC value. The figure indicates that increasing the channel width while keeping the exchanger length constant leads to a higher HTC value. For a 1 m exchanger length, the HTC increases by factors of 2.7, 6.8, and 12.9 with a 3, 6, and 9-fold increase in passage length. For a 0.15 m exchanger length, these values are 1.9, 3.77, and 6.33 times, respectively. It has been discovered that the HTC diminishes as the route lengthens in exchangers with shorter dimensions.

Figure 4 shows how the divider width, mass flow rate, average temperature, passageway width, and exchanger length all affect the pressure loss in a compact HEX. Figure 4(a) illustrates the relationship between pressure loss in a compact HEX and the dimensions of the divider and passageways. The diagram is determined using the following parameters: input air temperature of 300K, output air temperature of 400K, exchanger length of 0.15m, and air flow rate of 1 kg/s. The figure illustrates that pressure loss rises as the width of the divider and channels grows. For a passage width of 0.003 m, the pressure loss increases by 1.18, 1.38, 1.59, and 1.80 times when the divider thickness increases by 2, 3, 4, and 5 times. For a divider width of 0.04 m, these ratios are 1.06, 1.14, 1.21, and 1.28, respectively. It was noted that the rate of rise diminished as the passage width expanded.

Figure 4(b) illustrates the relationship between pressure loss in the compact HEX and the width of the divider, as well as the air mass flow rate values. The divider width was set at a constant value of 0.001 m, while the passage width was maintained at a constant value of 0.003 m during the figure construction. The graphic illustrates that the pressure loss of the compact HEX rises as the width of the divider value grows. For an air flow rate of 1 kg/s, the pressure loss

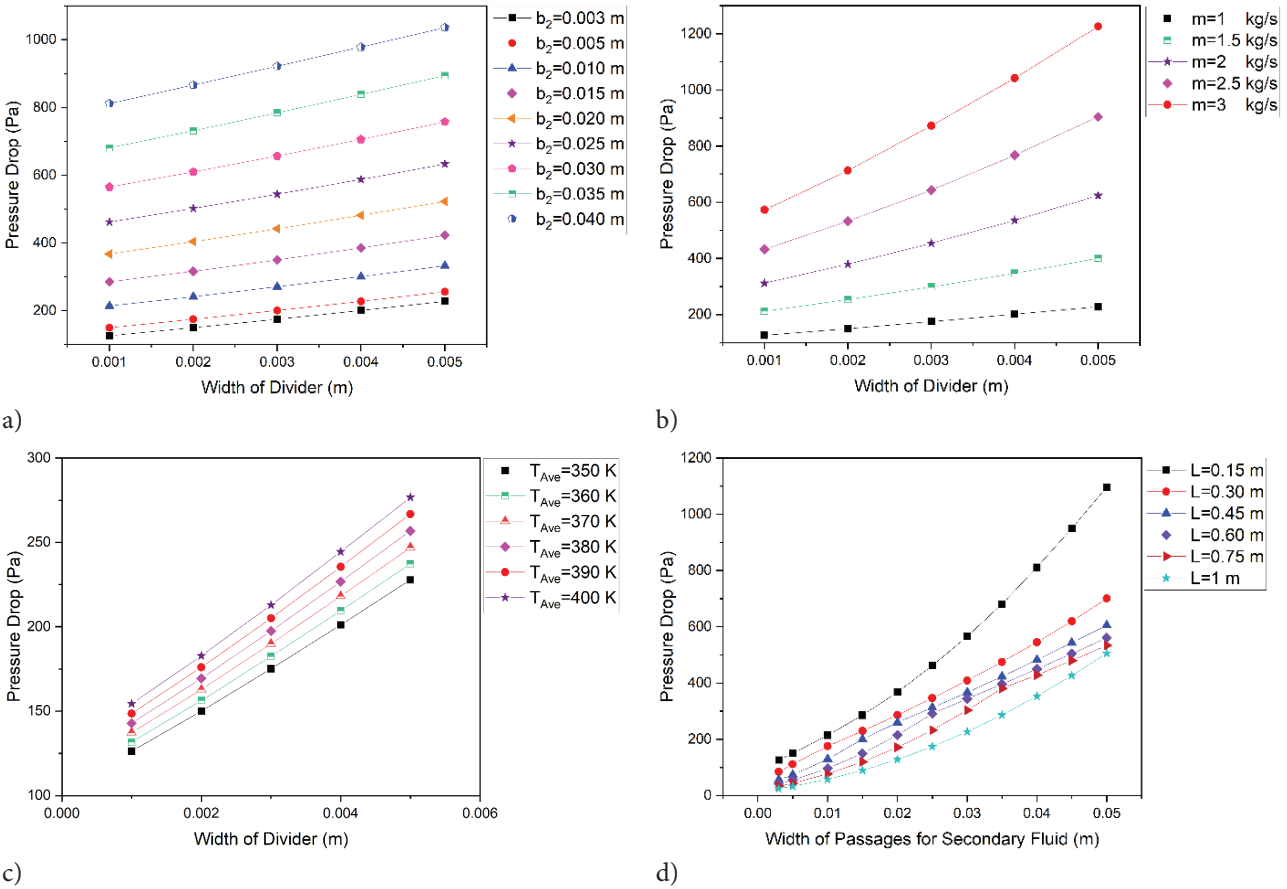

Figure 4. pressure drop variation with respect to a) length of heat exchanger, b) mass flow rate, c) average temperature, and, d) width of passages for secondary fluid.

increases by factors of 1.05, 1.12, 1.19, and 1.26 as the width of the divider is increased by 2, 3, 4, and 5 times, respectively. When the air flow rate is 3 kg/s, the pressure loss factors are 1.07, 1.14, 1.22, and 1.28 for the same increases in divider width. It is found that growth rates rise proportionally with an increase in air flow rate. The pressure loss change due to mass flow rate was computed as 1.25, 1.48, 1.70, and 1.89 times for a 0.001 m divider width and as 1.27, 1.51, 1.72, and 1.93 times for a 0.005 m divider width. It has been found that the pressure loss increases more significantly with larger dimensions of the divider width.

Figure 4(c) depicts the relationship between pressure loss in the compact HEX and the average air temperature across the divider's breadth. The figure was created with a constant air mass flow rate of 1 kg/s, an exchanger length of 1 m, and a passage width of 0.003 m. The figure illustrates that pressure loss rises as the width of the divider and the average temperature value increase. At an average air temperature of 350 K, the pressure loss value increases by factors of 1.18, 1.39, 1.59, and 1.80 as the width of the divider value increases by 2, 3, 4, and 5 times. When the average temperature is 400 K, these values change to 1.18, 1.38, 1.58, and 1.79 times, respectively. Changes in the average air temperature cause the pressure loss values for average air temperatures of 350 K and 400 K to go up by the same amount. For a divider width of 0.001 m, the pressure loss goes up by 1.04, 1.08, 1.13, 1.17, and 1.22 at different temperatures. For a divider width of 0.005 m, the pressure loss goes up by 1.04, 1.08, 1.12, 1.17, and 1.21 at different temperatures. The consequences display that changing the

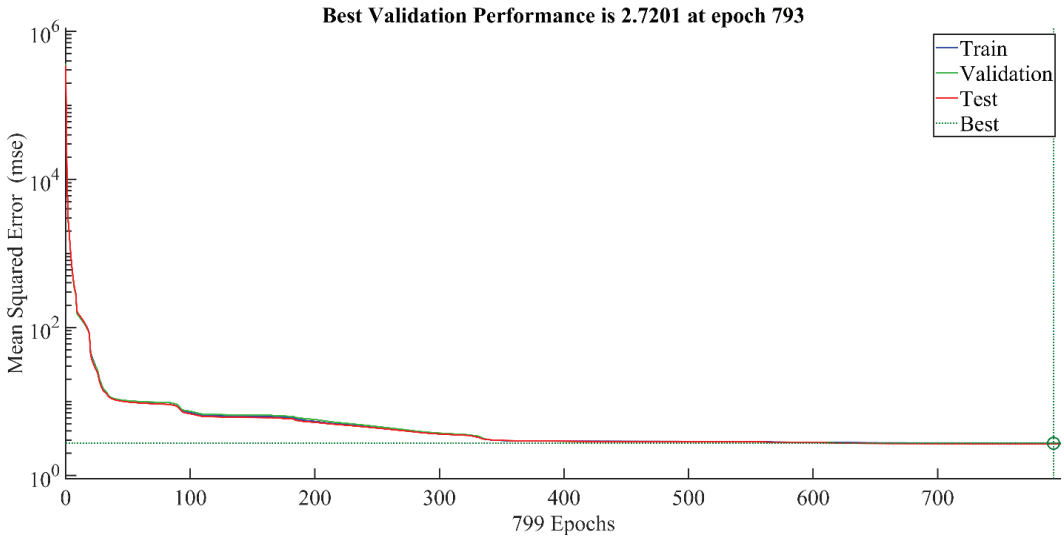

(a)

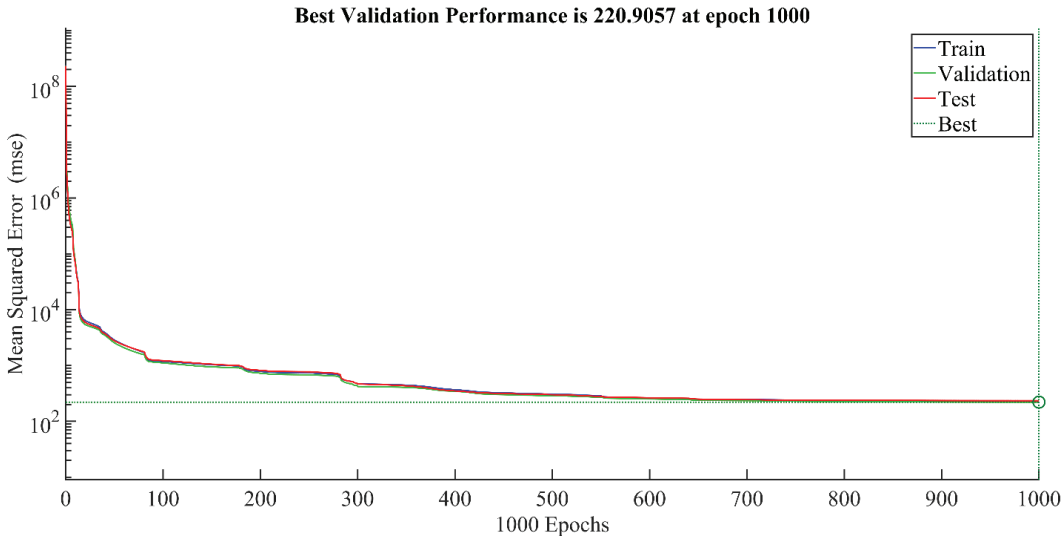

(b)

Figure 5. The training performance of the ANN model in model for (a) heat transfer coefficient, (b) pressure drop.

width of the divider has slight outcome on the ΔP when the average temperature stays the same.

Figure 4(d) displays the pressure loss value variation in the compact HEX based on the width of the channel and the exchanger length. When designing this figure, the divider width was maintained at a constant value of 0.001 m, with an air input temperature of 300 K, an air output temperature of 400 K, and an air flow rate of 1 kg/s. The figure demonstrates that the pressure loss goes up as the channel gets wider and the exchanger length value goes down. The pressure loss values for passage widths of 0.015, 0.03, and 0.045 m increased by 1.98 and 3.32 times when the exchanger length was 0.15 mm. When the exchanger length was 1 m, they increased by 2.53 and 4.75 times. The results show that the pressure loss increases as the length of the exchanger increases, especially when the width of the passage changes.

It was determined whether the training stage of the ANN structure was carried out appropriately by analyzing the training performance. The outcomes of the ANN training are illustrated in Figure 5(a) for HTC and in Figure 5(b) for ΔP, respectively. In spite of initially large MSEs throughout training the ANN architecture, they shrank with time. An epoch in MLP networks is a cycle in which data is directed after the output layer to the input layer to lower the number of errors. The MLP method that use this study are named feed-forward backpropagation (FF-BP) NN methods. The HTC model finished training afterward epoch 793, and the ΔP model finished later epoch 1000. The MSE values went down with each stage of training, validation, and testing. Figure 5 shows that the NN has finished its training. When training an ANN, it is important to look at the error histograms, which show the differences among the modeled and real results, to figure out where the training errors are coming from.

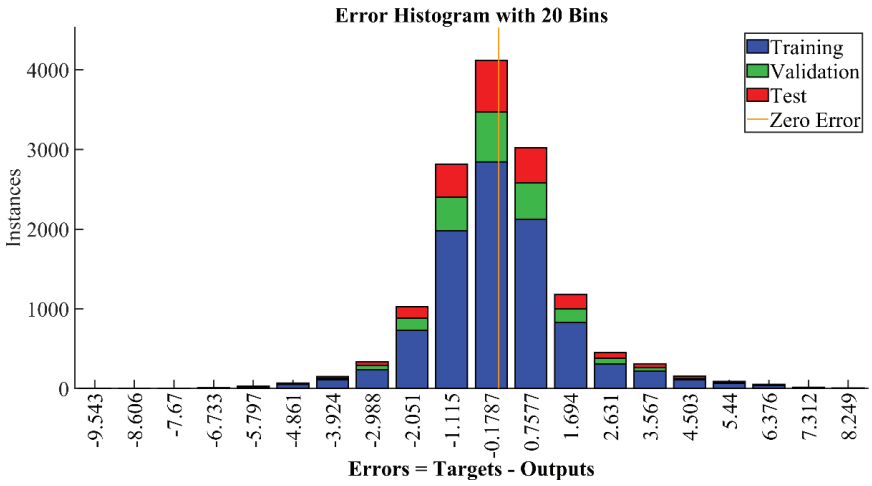

(a)

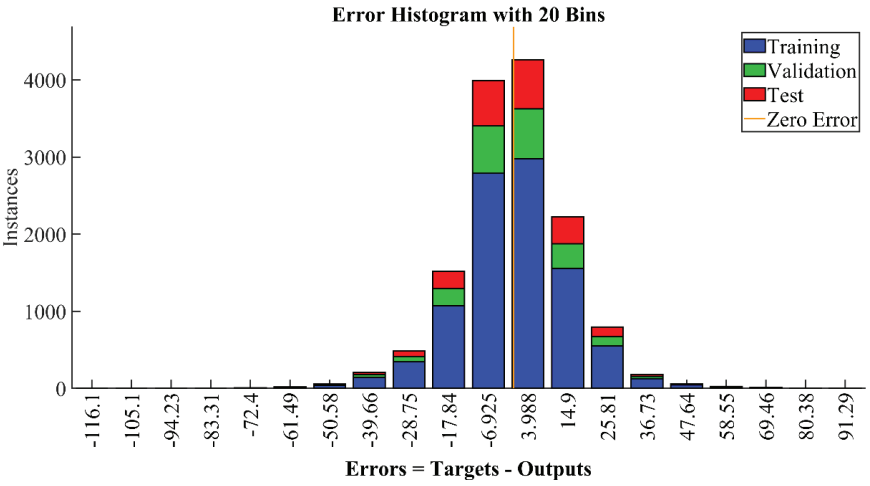

(b)

Figure 6. Error histogram for ANN model for a) heat transfer coefficient, and b) pressure drop.

The error histogram of the ANN model is shown in Figure 6. When we looked at the error histogram, we saw that the estimated error data for all three values were very near to the yellow line, which meant that there was no inaccuracy. Also, there are very few mistakes in the abscissa. The error histogram for the ANN model shows that the NN study's training stage was done correctly, with only a few mistakes. The MSE for heat transfer and ΔP was -0.1787 and 3.988, respectively. The results show that the ANN's training stage, which was meant to predict the heat transfer and ΔP values, went perfectly.

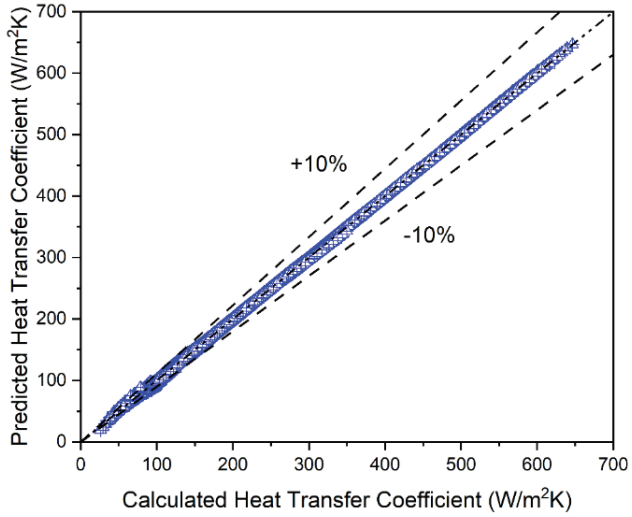

(a)

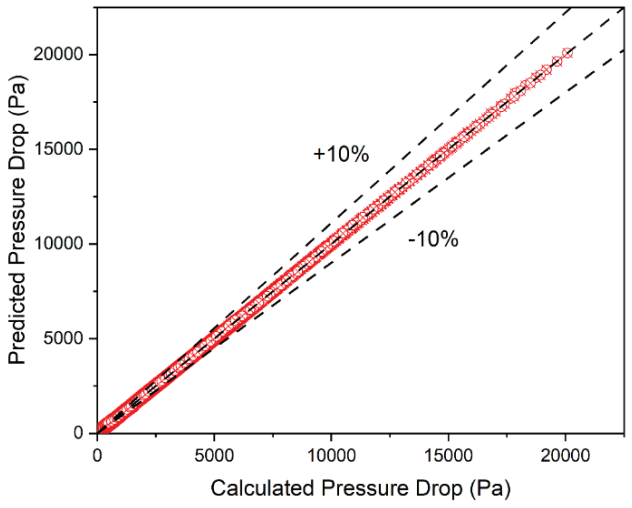

(b)

Figure 7. Target and prediction values in ANN model for (a) heat transfer coefficient, and (b) pressure drop

Figure 7(a)-(b) displays target and estimated measurements for two scenarios involving HTC and ΔP. The goals are on the x-axis, and the ANN predictions are on the y-axis. The data points for the two ANN models are either very close to zero or on a straight line. The consequences show that the data points have a margin of error of plus or minus 10 percentage points. The figures show that predicted values for HTC exceeding 200 W/m²K and ΔP surpassing 5000 Pa are within ±10 margins, whereas values below these thresholds are within ±15 margins. Table 3 details the consequences of two separate ANN representations created to forecast NN values in numerous situations. The MoD values calculated for ANN methods were found to be very low.

Figure 8 shows the MoD values, which show how different the ANN model-generated output values are from the theoretical calculations. An examination of the 13860 generated data points indicates that the majority are situated along the error line, in proximity to zero. This has become clear as we've looked at the data. Because the MoD values are so close to the line, which means 0% error, it means that the differences between the values of HTC and ΔP that the ANN and the theoretical data give are very small. It has been found that the average MoD values for heat transfer and ΔP are -0.003% and 0.0582%, respectively. The lowest values for the given parameters are -0.13% and -0.189%, and the highest values are 0.249% and 3.394%. The MoD value analysis shows that the MLP NN that is used can make very accurate predictions about the outputs of the compact plate HEX. These results are obtained by analyzing the MoD values.

A thorough error analysis of the ANN methods was performed by calculating the variances among the method results and the target data for each data point, as illustrated in Figures 9a–b. Figure 9a illustrates the differences among ANN outputs and the necessary HTC, while Figure 9b presents the ΔP. The deviations in HTC and ΔP productions after the anticipated values are given in Figure 9. The figures show the minimum, maximum, and average values of the target-prediction parameter for HTC are -10.01, 8.717, and 0.00078, respectively. These numbers are -121.50, 96.74, and 0.0978 for ΔP. The outputs generated by four

Table 3. MoD values for both ANN models in heat transfer coefficient and pressure drop

	MoD (%)			MSE	MAPE	R
	Min	Max	Ave			
for Heat Transfer Coefficient	-0.13	0.249	-0.003	2.046	0.00746	0.999
for Pressure Drop	-0.189	3.394	0.0582	173.85	0.02045	1

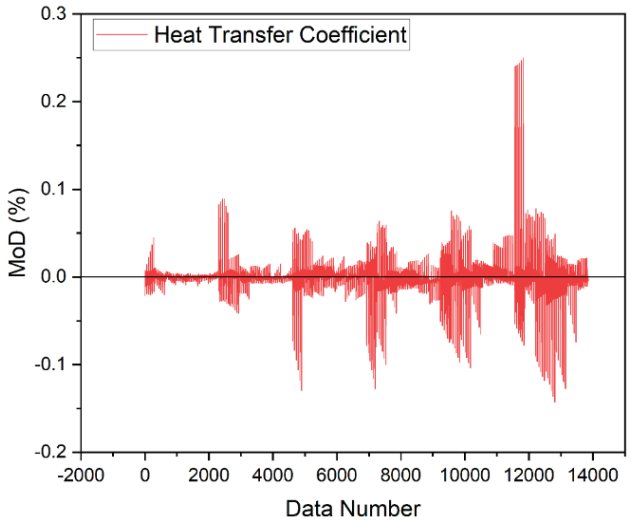

(a)

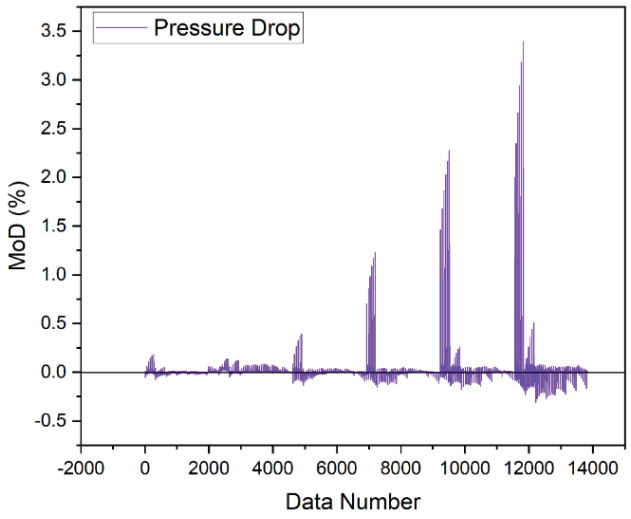

(b)

Figure 8. The calculated MoD values for each data point in ANN model for (a) heat transfer coefficient, and (b) pressure drop.

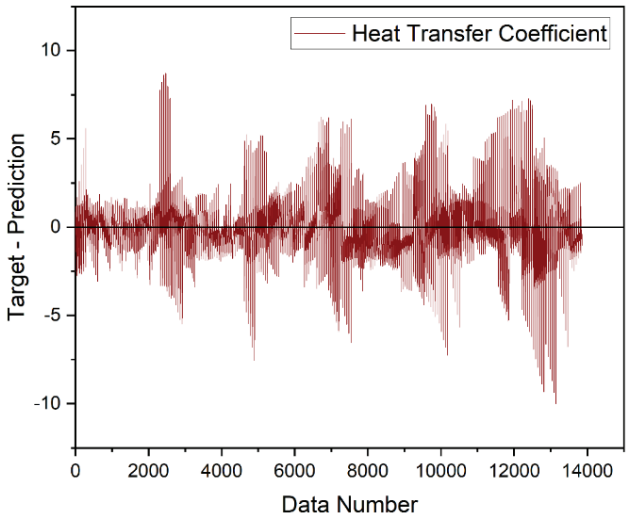

(a)

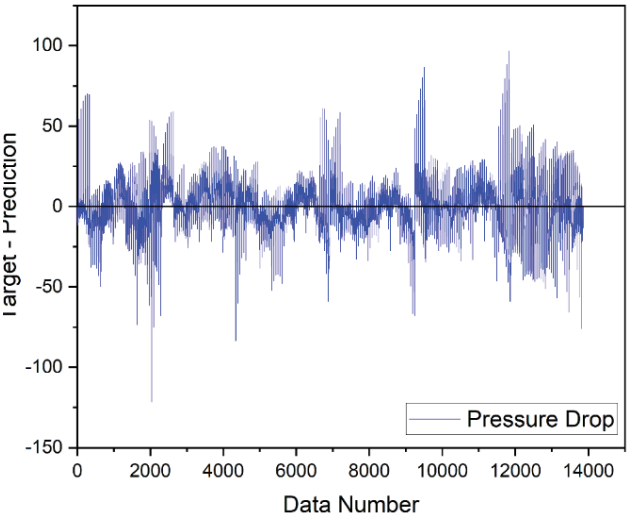

(b)

Figure 9. The differences between target values and ANN outputs in ANN model for (a) heat transfer coefficient, and (b) pressure drop.

distinct ANN models exhibit considerable similarity. The Ministry of Defense and the deviation results show that the two artificial neural network models can give neural network values with moderate standard deviations.

The MAPE values for HTC and P are shown in Figure 10. The minimum, maximum, and average MAPE values for the HTC parameter are 4.082E-07, 0.2495, and 0.00967, respectively. For ΔP, the corresponding values are determined as 1.733E-06, 3.394, and 0.02535.

CONCLUSION

This study examines the efficiency of a plate-type compact HEX in heat transfer and the pressure loss relative to its design specifications. It then looks at how those results compare to those found using the Levenberg-Marquardt artificial neural network method. To get the air inlet and output temperatures to change while keeping the atmospheric pressure and fin thickness the same, the designers had to think about a lot of different things, like the air flow rate, the width of the divider, the width of the route, and the length of the compact heat exchanger. The study produced the following results:

1. The study shows that the heat transfer coefficient in heat exchangers goes up as the channel width and air mass flow rate go up. On average, they go up by 51.3% and 93%, respectively. The coefficient also increases naturally with increasing air temperature, with a divider

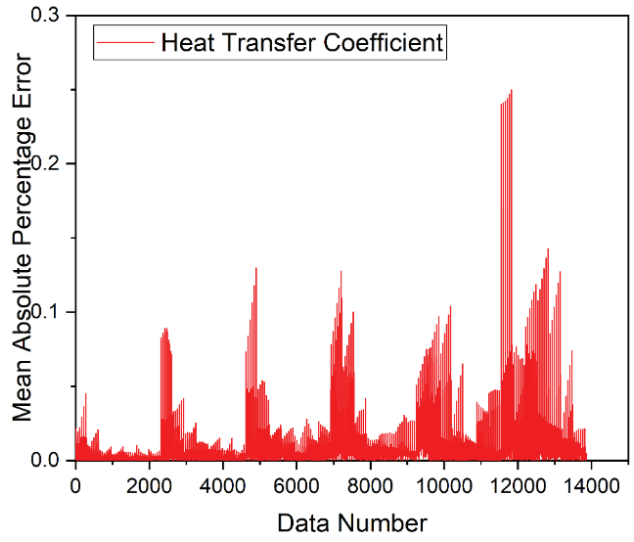

(a)

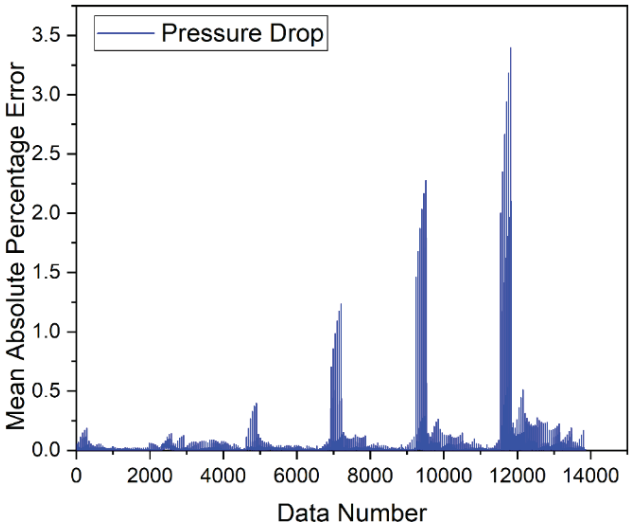

(b)

Figure 10. Mean absolute percentage error in ANN model for (a) heat transfer coefficient, and (b) pressure drop.

width of 0.001 m resulting in a 7.9% increase. Increasing channel width while maintaining exchanger length leads to higher heat transfer coefficient values.

2. The study reveals that increasing divider thickness leads to higher pressure loss, but the rate of rise decreases with passage width. Pressure drops factors increase proportionally with air flow rate, with growth rates rising proportionally with divider width. Larger divider width sizes make pressure loss worse. As the average air temperature changes, the pressure drops more, and the divider widths of 0.001 m and 0.005 m show similar increases. But the width of the divider has little effect on the drop in pressure.
3. The training phase of the ANN successfully estimated heat transfer and pressure drop values, with MSE values of -0.1787 and 3.988, respectively.
4. The study found that the predicted values for heat transfer coefficient and pressure drop are within a ±10 margin, while values below these thresholds are within a ±15 margin.
5. The MoD value analysis reveals that the MLP NN, which is implemented, accurately predicts the outputs of the compact plate heat exchanger, with average values of -0.003% and 0.0582%.
6. The heat transfer coefficient parameter has MAPE values of 4.082E-07, 0.2495, and 0.00967, while the pressure drop has MAPE values of 1.733E-06, 3.394, and 0.02535.

NOMENCLATURE

A	*Area [m²]*
b	*Width of passages [m]*
cp	*Specific heat [J/kg.K]*
D	*Diameter [m]*
DP	*Pressure drop [Pa]*
f	*Fanning friction factor*
G	*Mass flux [kg/m²]*
g	*Proportionality factor in Newton's second law*
h	*Heat transfer coefficient [W/m²K]*
j_H	*Colburn factor*
l	*Fin length [m]*
m	*Fin effectiveness parameter*
$\dot{m}$	*Mass flow rate [kg/s]*
n	*Efficiency*
Nu	*Nusselt number*
p	*Fin pitch [m]*
Pr	*Prandtl number*
q	*Heat transfer capacity [W]*
Re	*Reynolds number*
St	*Stanton number*
T	*Temperature [K]*
U	*Total heat transfer coefficient [W/m²K]*
v	*Velocity [m/s]*
X	*Data*
δ	*Width of divider [m]*
δ_f	*Fin thickness [m]*
ε	*Effectiveness*
σ	*Ratio of the free flow area to the frontal area indices*
Ave	*Average*
c	*cold*
$Calc$	*Calculated*
f	*Front*
f	*Fin*
fr	*Frontal*
h	*hot*
h	*Hydraulic*
in	*Inlet*
max	*Maximum*

min *Minimum*
o *Overall*
out *Outlet*
p *Constant pressure*
tot *Total*
w *Wall*

Abbreviations

ANN	Artificial neural network
CFD	Computational fluid dynamics
CHE	Compact heat exchanger
GA	Genetic algorithm
HEX	Heat exchanger
HTC	Heat transfer coefficient
MAPE	Mean absolute percentage error
MLP	Multilayer perceptron
MoD	Margin of deviation
NN	Neural network
MSE	Mean squared error
PCHE	Printed circuit heat exchanger
PFHE	Plate fin heat exchanger

DATA AVAILABILITY STATEMENT

The authors confirm that the data that supports the findings of this study are available within the article. Raw data that support the finding of this study are available from the corresponding author, upon reasonable request.

CONFLICT OF INTEREST

The author declared no potential conflicts of interest with respect to the research, authorship, and/or publication of this article.

ETHICS

There are no ethical issues with the publication of this manuscript.

STATEMENT ON THE USE OF ARTIFICIAL INTELLIGENCE

Artificial intelligence was not used in the preparation of the article.

REFERENCES

[1] Ermis K. ANN modeling of compact heat exchangers. Int J Energy Res 2008;32:581–594. [CrossRef]
[2] Demir MH. Thermal Modeling and Performance Analysis for a Chevron Type Heat Exchanger by Using Artificial Neural Network with Limited Experimental Data. Eur J Sci Technol 2020;18:779–789.
[3] Shi H, Chang H, Ma T, Wang Q. Prediction of Equivalent Thermal Conduction Resistance of Printed Circuit Heat Exchangers. J Therm Sci 2022;31:2281–2292. [CrossRef]
[4] Dossumbekov YK, Zhakiyev N, Nazari M A, Salem M, Abdikadyr B. Sensitivity Analysis and Performance Prediction of a Micro Plate Heat Exchanger by Use of Intelligent Approaches. Int J Thermofluids 2024;100601. [CrossRef]
[5] Jiang T, Li MJ, Yang JQ. Research on optimization of structural parameters for airfoil fin PCHE based on machine learning. Appl Therm Eng 2023;229:120498. [CrossRef]
[6] Zhu G, Wen T, Zhang D. Machine learning based approach for the prediction of flow boiling/condensation heat transfer performance in mini channels with serrated fins. Int J Heat Mass Transf 2021;166:120783. [CrossRef]
[7] Zarea H, Kashkooli FM, Mehryan AM, Saffarian MR, Beherghani EN. Optimal design of plate-fin heat exchangers by a Bees Algorithm. Appl Therm Eng 2014;69:267–277. [CrossRef]
[8] Hernández-Gil JA, Colorado-Garrido D, Alaffita-Hernández FA, Escobedo-Trujillo BA. Heat exchanger design considering variable overall heat transfer coefficient: An artificial neural network approach. Heat Transfer 2022;51:2488–2509. [CrossRef]
[9] Zeng M, Du LX, Liao D, Chu WX, Wang QW, Luo Y, et al. Investigation on pressure drop and heat transfer performances of plate-fin iron air preheater unit with experimental and Genetic Algorithm methods. Appl Energy 2012;92:725–732. [CrossRef]
[10] Gupta D, Saha P, Roy S. Multi-Objective Optimization of Air-Cooled Perforated Micro-Pin Fin Heat Sink Via an Artificial Neural Network Surrogate Model Coupled With NSGA-II. J Therm Sci Eng Appl 2024;16:011004. [CrossRef]
[11] Peng H, Ling X. Predicting thermal–hydraulic performances in compact heat exchangers by support vector regression. Int J Heat Mass Transf 2015;84:203–213. [CrossRef]
[12] Peng H, Ling X. Neural networks analysis of thermal characteristics on plate-fin heat exchangers with limited experimental data. Appl Therm Eng 2009;29:2251–2256. [CrossRef]
[13] Nascimento CAR, Mariani VC, Coelho LS. Integrative numerical modeling and thermodynamic optimal design of counter-flow plate-fin heat exchanger applying neural networks. Int J Heat Mass Transf 2020;159:120097. [CrossRef]
[14] Xie C, Yan G, Ma Q, Elmasry Y, Singh PK, Algelany AM, et al. Flow and heat transfer optimization of a fin-tube heat exchanger with vortex generators using Response Surface Methodology and Artificial Neural Network. Case Stud Therm Eng 2022;39:102445. [CrossRef]
[15] Xie GN, Sundén B, Wang QW. Optimization of compact heat exchangers by a genetic algorithm. Appl Therm Eng 2008;28:895–906. [CrossRef]

[16] Jilak A, Assareh E, Nedaei M. Application of a novel multi-objective optimisation method integrated with the artificial neural networks for optimum design of a plate heat exchanger. Australian J Mech Eng 2017;1–15. [CrossRef]

[17] Peng H, Ling X. Optimal design approach for the plate-fin heat exchangers using neural networks cooperated with genetic algorithms. Appl Therm Eng 2008;28:642–650. [CrossRef]

[18] Kays WM, London AL. Compact heat exchangers. Florida; Krieger Publishing Company; 1984.

[19] Gardner KA. Efficiency of extended surface. Trans American Soc Mech Eng 1945;67:621–628. [CrossRef]